Indian Journal of Pure & Applied Physics
Vol. 60, June 2022, pp. 489-496

Parametric Study of CPT Resonance in Rubidium Vapor Cell for Application in Atomic Clock

Rajaiah Kaitha[a*], Manjula R[b], Pragya Tiwari[b], Minni J Kappen[b], Shubhajit Biswas[b], Bijoy Raha[b], Swarupananda Pradhan[c], Venkatappa Rao Tumu[d*], Umesh S B[b], Elumalai S[b], Kalpana Arvind P[b], Sriram K V[b] & Prashanth C Upadhya[b]

[a]U.R. Rao Satellite Centre, Indian Space Research Organisation, Bangalore-560 017, India
[b]Laboratory for Electro-Optics Systems, Indian Space Research Organisation, Bangalore-560 058, India
[c]Bhabha Atomic Research Centre, Mumbai-400 085, India
[d]Department of Physics, National Institute of Technology, Warangal, Telangana-506 004, India

Received 11 March 2022; accepted 6 May 2022

The performance of Coherent Population Trapping (CPT) based atomic clocks primarily depends on the characteristics of CPT resonance. We have performed experiments to study and optimize the characteristics of CPT resonance in ^{87}Rb atoms by measuring its contrast and full-width-at-half maximum (FWHM) as function of laser excitation and temperature of atomic vapor cells with different dimensions. A four-level atomic model is used to simulate CPT resonance characteristics along the length of atomic vapor cell. The model incorporates scaling law to understand collision dynamics in cells with different radius for a range of laser excitation intensities and the results are compared with experimental data. The quality figure, calculated from the measured values of FWHM and contrast, decreases with increase in laser intensity and improves in cells with higher dimension (radius). The optimum temperature corresponding to maximum quality figure varies with laser excitation intensity as well as cell dimension. The underlying collision dynamics and density effects that are responsible for the observed resonance characteristics are discussed.

Keywords: Atomic clock; Coherent Population Trapping; Quality figure; Frequency stability; Wall collision; Propagation effect

1 Introduction

Coherent Population Trapping is a quantum interference phenomenon which is an alternate technique to develop atomic clocks using alkali atoms. Particularly, CPT phenomenon in Rubidium (Rb) and Cesium (Cs) atoms is widely employed in realizing vapor cell based miniature atomic clocks[1-3]. Short term frequency stability of these clocks depends primarily on the quality figure (q) which depends on the characteristics of CPT resonance, *i.e.*, its amplitude and FWHM (linewidth). Quality figure is defined as the ratio of contrast (C) and linewidth ($\Delta\nu_{FWHM}$) of CPT resonance. Contrast is defined as the ratio of resonance amplitude (dI) to the background current (I_{bg}). In order to improve the frequency stability of atomic clock it is imperative that CPT resonance would need to be optimized with higher q value[4]. However, the characteristics of CPT resonance are determined by the nature of laser-atom interaction in an atomic vapor cell that depends on variety of factors, viz. laser intensity[3], cell temperature[5,6], cell dimension[5,7], buffer gas species and its pressure in the atomic cell[8-11]. In atomic clocks based on alkali vapor cells, buffer gas is used to reduce the ground state relaxation[12].

For a symmetric three level (Λ-configuration) atomic system, linewidth ($\Delta\nu_{FWHM}$) of the CPT resonance is given by[3],

$$\Delta\nu_{\mathrm{FWHM}} = \frac{1}{\pi}\left(\gamma_2 + \frac{{\omega_R}^2}{\Gamma^*}\right) \qquad \ldots(1)$$

where γ_2 and Γ^* are the ground state coherence relaxation rate and excited state decay rates, respectively; ω_R is Rabi frequency which indicates the strength of laser-atom interaction and proportional to laser excitation intensity.

The amplitude of CPT resonance primarily depends on the number of atoms participating in CPT phenomena which is function of cell temperature, length, and laser beam diameter[5,13]. The laser excitation intensity would affect the Rabi frequency of atomic transition which influences both amplitude of CPT resonance as well as its FWHM[14,15]. FWHM also depends on the coherence relaxation rates of ground and excited states[14]. Particularly, the ground

*Corresponding authors: (Email: krajaiah@ursc.gov.in; tvraokmm@nitw.ac.in)

state relaxation (γ_2) is influenced by collisional interactions in the vapor cell, viz. collision between alkali atoms-buffer gas (γ_{2BG}), alkali-alkali atoms or spin-exchange collision (γ_{2SE}) and alkali atoms-cell wall (γ_{2W})[3]. The alkali atoms-cell wall collisions are highly influenced by the cell dimension. Thus, the contrast and FWHM of CPT resonance depend on critical operating parameters, *i.e.*, laser excitation intensity and temperature as well as dimension of atomic vapor cell. Therefore, formulating a suitable scaling law based on theoretical model that is in accordance with the practical observation of the characteristics of CPT resonance, is of paramount interest for improving the frequency stability of CPT based atomic clock. Furthermore, the validation of theoretical model with experimental observations is essential for fixing the tolerance of critical operating parameters within the limits of design constraint.

In this paper, we have used a four-level atomic model for computing CPT resonance in cells with different size (radius) which are excited at different laser intensities. We have introduced a new parameter in the model to account for the influence of cell size on resonance characteristics and compared with the experimental results. The theoretical limit of cell length where the quality figure saturates is predicted for different laser intensities. Further, the variation of optimum temperature corresponding to maximum quality figure is studied with respect to laser intensity and cell dimension.

2 CPT Resonance – Theoretical Model

Theoretical analysis is carried out by modelling the evolution of laser-atom interaction in atomic ensemble along the length of the atomic vapor cell. CPT resonance is simulated by estimating the variation of Rabi frequency corresponding to the D1 hyperfine transition in ^{87}Rb atoms as function of Raman detuning frequency.

The Rabi frequency of a given atomic transition is proportional to amplitude of laser radiation[16].

$$\omega_R = \left(\frac{E_0}{\hbar}\right) < i|\boldsymbol{er}.\boldsymbol{e_\lambda}|j > \qquad \ldots(2)$$

Here, E_0 is amplitude of laser radiation and $\hbar$ is modified Planck's constant and $< i|\boldsymbol{er}.\boldsymbol{e_\lambda}|j > = d_{ij}$ is the electric dipole matrix element of the transition from ground state i to excited state j. Using the relation $I_L = \frac{1}{2}c\varepsilon_0 {E_0}^2$ (Ref. (17)), the equation for Rabi frequency can be expressed as:

$$\omega_R = \sqrt{\frac{2I_L {d_{ij}}^2}{c\varepsilon_0\hbar^2}} \qquad \ldots(3)$$

Rabi frequency changes as function of laser excitation intensity (I_L) and Eq. (3) provides the Rabi frequency corresponding to the incident laser light at the entrance of the cell. Rabi frequency varies along the length of vapor cell (propagation length) when laser frequency is tuned to CPT resonance as CPT phenomena changes light absorption in the cell. Furthermore, for application in atomic clocks, the propagation effect is of concern since clocks are operated at relatively higher temperature for improving the amplitude of the signal which results in larger Rb density that affects the Rabi frequency. Hence, for each incident laser excitation intensity, the resulting CPT resonance is modelled by estimating the Rabi frequency of corresponding transmitted laser light through the vapor cell as function of Raman detuning. The resonance characteristics are then extracted by performing suitable curve fit.

It may be noted that when atomic vapor cells are operated at elevated temperatures and relatively higher laser excitation intensity, the atomic medium in the vapor cell becomes optically thick. For conventional operating conditions, the CPT resonances need to be modelled using a four-level atomic system[3] which is shown in Fig. 1. The collisions between buffer gas atoms and Rb atoms cause the decay of excited state atoms to all possible ground state Zeeman levels. Under circular polarization σ^+ (or σ^-) the transitions from $m_F = +2$ (or $m_F = -2$) are forbidden *i.e.*, the atoms in these states do not contribute to CPT phenomenon. These trapped atoms are represented by a fourth level known

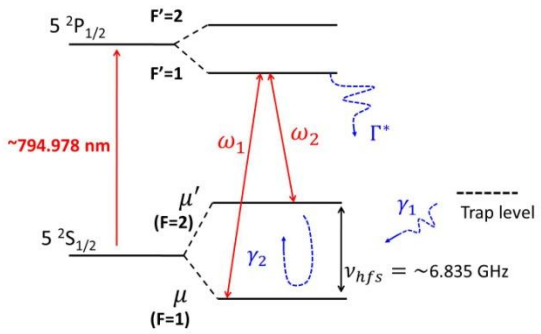

Fig. 1 — Four level atomic system used in the theoretical calculation of CPT resonance. The trap level indicates the fourth level which represents the trapped atoms that do not contribute to CPT phenomena.

as "trap level"[3,16] as shown in Fig. 1. The three-level model with this trap is called as four level atomic system.

With four level model, characteristics of CPT resonance can be studied by estimating the variation in Rabi frequency of laser light due to absorption along the length of vapor cell which is represented by Eq. (4)[3,18].

$$\frac{\partial \omega_R}{\partial z} = \alpha \, Im\delta_{\mu m} \qquad \ldots(4)$$

Where, α is absorption coefficient and $Im\delta_{\mu m}$ is imaginary part of the density matrix element in which $\delta_{\mu m}$ describes the induced coherence in the atomic medium due to laser excitation. $Im\delta_{\mu m}$ is given by Eq. (5)[3]

$$Im\delta_{\mu m} = -\frac{\omega_R(z)}{\Gamma^*}\left[\frac{1}{3} - \frac{\left(\frac{2}{9}\right)\frac{\omega_R^2(z)}{2\Gamma^*\gamma_1}}{1+\left(\frac{2}{3}\right)\frac{\omega_R^2(z)}{2\Gamma^*\gamma_1}} + \delta^r_{\mu\mu'}\right] \qquad \ldots(5)$$

Where, $\delta^r_{\mu\mu'}$ is the real part of the ground state coherence. By substituting the expression for $\delta^r_{\mu\mu'}$ as described in Ref. (3), the variation in Rabi frequency can be written as shown in Eq. (6).

$$\frac{\partial \omega_R}{\partial z} = -\beta\alpha\frac{\omega_R(z)}{\Gamma^*}\left[\frac{1}{3} - \frac{\left(\frac{2}{9}\right)\frac{\omega_R^2(z)}{2\Gamma^*\gamma_1}}{1+\left(\frac{2}{3}\right)\frac{\omega_R^2(z)}{2\Gamma^*\gamma_1}} - \frac{\left(\frac{2}{3}\right)\frac{\omega_R^2(z)}{2\Gamma^*}\left(\gamma_2+\frac{\omega_R^2(z)}{\Gamma^*}\right)+\left(\frac{4}{9}\right)\frac{\frac{\omega_R^4(z)}{4\Gamma^{*2}}(\gamma_2+\frac{\omega_R^2(z)}{\Gamma^*})}{\gamma_1(1+\frac{\omega_R^2(z)}{3\Gamma^*\gamma_1})}}{(\gamma_2+\frac{\omega_R^2(z)}{\Gamma^*})^2+(\omega_{12}-\omega_{\mu'\mu})^2}\right] \qquad \ldots(6)$$

where Γ^* decay rate of excited state
$\omega_R(z)$ Rabi frequency at a position z along the length of vapor cell
γ_1 relaxation rate of ground state population
γ_2 relaxation rate of ground state coherence and is the measure of collisional interactions in the atomic vapor cell
ω_1, ω_2 angular frequencies of laser sidebands $(\omega_{12} = \omega_1 - \omega_2)$
$\omega_{\mu'\mu}$ angular frequency of hyperfine ground state

The term β is cell dimension (radius) dependent scale factor ($\beta = a_0 + a_1R + a_2R^2$; where R is cell radius and a_0, a_1, a_2 are constants).

The parameter β has been introduced to account for the effect of cell size (radius) on CPT resonance. Analytical solution for Eq. (6) is not possible as it is highly non-linear and complex. So, RK4 (Range-Kutta 4th order) numerical integration method has been employed to calculate the Rabi frequency along the length of vapor cell. For each incident laser intensity, the Rabi frequency at any position (z) along the length of vapor cell is given by

$$\omega_R(z = l) = \omega_R(z = l - \delta l) + \delta\omega_R \qquad \ldots(7)$$

where $\delta\omega_R = \frac{\delta l}{6}(k_1 + 2k_2 + 2k_3 + k_4)$ and k_1, k_2, k_3, k_4 are intermediate slopes of integrating function

$k_1 = f(\omega_R(z = l - \delta l)) = \frac{\partial \omega_R(z=l-\delta l)}{\partial z}$,
$k_2 = f\left(\omega_R(z = l - \delta l) + \frac{\delta l}{2}k_1\right)$,
$k_3 = f\left(\omega_R(z = l - \delta l) + \frac{\delta l}{2}k_2\right)$,
$k_4 = f(\omega_R(z = l - \delta l) + \delta l k_3)$.

δl is the incremental length of vapor cell (δl =1 mm in our calculation) and $l = 1\delta l, 2\delta l, 3\delta l, \ldots\ldots, L$. Rabi frequency at the exit of a vapor cell with length L (*i.e.*, $\omega_R(z = L)$) is then calculated through the iterative process by considering $l = \delta l$ to L. The values of γ_2 and Γ^* are extracted from the fitted experimental data using Eq. (1) and an approximation of $\gamma_1 = \gamma_2$ is used in our theoretical calculation[16]. Fig. 2 shows the computed Rabi frequencies with respect to Raman detuning for cells (radius, R ~ 12.5 mm; temperature, T ~ 71 ^{0}C; $\gamma_2 = 630\,\frac{rad}{s}$ and $\Gamma^* = 1.5 \times 10^{10} s^{-1}$) with different lengths (L) which represent the corresponding CPT resonances.

The quality figure 'q' is calculated by extracting contrast and FWHM using Lorentzian fit to the computed CPT resonance. The q values of CPT resonances in cells with lengths up to 300 mm under

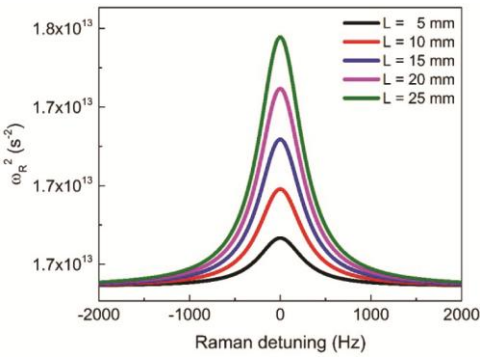

Fig. 2 — Rabi frequencies (CPT resonance) computed by numerical integration of Eq. (6) for cells with lengths (L). The amplitude of CPT resonances increases and FWHM decreases with cell length.

various laser excitation intensity values are calculated and plotted in Fig. 3. For smaller cell lengths (< 30 mm), the q increases with excitation intensity at lower intensity values and decreases with increase in intensity at higher values as a result of power broadening. However, the quality figure saturates beyond a threshold value of cell length. The saturation length becomes longer and quality figure tends to increase non-linearly for higher excitation intensities. The theoretical calculation shows that the observed quality figure as function of cell length and excitation intensity primarily depends on variation in contrast. However, the longer cells at higher excitation intensities, though results in superior quality figure, may not be suitable for application in space borne atomic clock. Moreover, light intensity dependent light shift effect could also become dominant contributor to medium as well as long-term frequency instability[19,20].

3 Experiment

The functional block diagram of CPT scheme employed in this study is as depicted in Fig. 4. The ʌ-system used in this experiment is formed by the D1 transitions ($5^2S_{1/2} \rightarrow 5^2P_{1/2}$) in ^{87}Rb atoms in which the two hyperfine ground states (F=1 and 2) couple to a common excited state (F'=1). A Vertical Cavity Surface Emitting Laser (VCSEL) diode emitting light ~ 794 nm is used to produce two coherent optical fields by means of current modulation such that the frequency difference between these two coherent optical fields is equal to the separation between hyperfine ground states. This is achieved by modulating VCSEL's injection current at radio frequency (RF) that corresponds to half the transition frequency ($\nu_{hfs}/2$ ~ 3.417 GHz) between hyperfine ground states of ^{87}Rb atoms. A phase lock loop (PLL) synthesizer seeded by a crystal oscillator (@ 10 MHz) is used for generating the RF. The collimated laser light with beam diameter ~3 mm first passes through a neutral density (ND) filter in order to change the laser intensity to a desired value. The attenuated laser light then passes through a quarter-wave (λ/4) plate which converts the polarization of light from linear to circular for state selection.

The circularly polarized light passes through a Pyrex vapor cell containing natural Rb (^{85}Rb + ^{87}Rb) and Ne as buffer gas at a pressure, P = 50 torr. The transmitted light is then detected by a silicon photo detector. Magnetic field is applied along the laser beam direction using a solenoid coil for exciting CPT among field independent Zeeman lines ($m_F = 0$). Laser emission frequency is stabilized by locking its frequency to a chosen atomic hyperfine transition using correction signal by employing Phase Sensitive Detection (PSD) and servo locking system as shown in Fig. 4. This has enabled us to minimize the adverse effects of laser instabilities on CPT resonance.

When the RF modulation frequency is scanned such that the first order side bands in the emitted laser field are resonant with two ground state hyperfine transitions of ^{87}Rb atoms, CPT resonance is observed. As shown in Fig. 4, the output frequency of crystal oscillator, when stabilized with respect to the CPT resonance, would serve as clock output. This study is focused on practical ways to optimize the operating parameters that would affect the CPT resonance which in turn impact the stability of atomic clock.

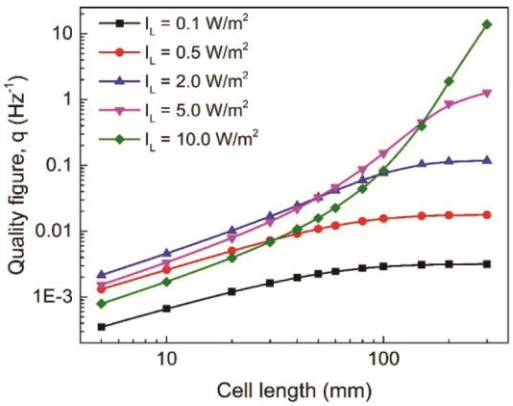

Fig. 3 — Variation of quality figure of CPT resonance with cell length for different incident laser excitation intensities.

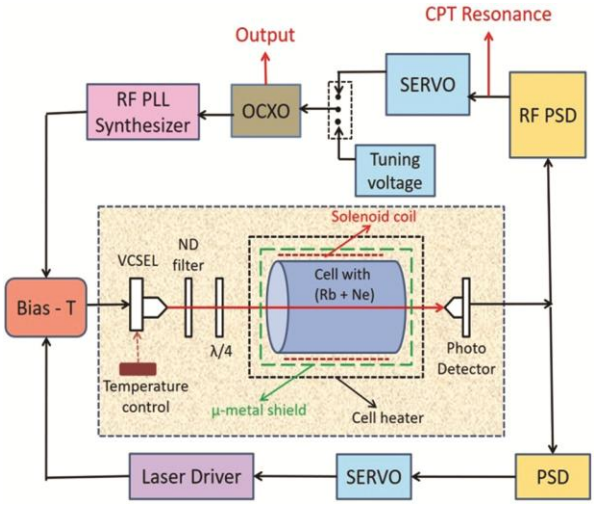

Fig. 4 — Functional block diagram of CPT scheme employed in this study.

The characteristics of CPT resonance are investigated experimentally by measuring its q by varying laser excitation intensity and the temperature of vapor cell with different radius but all with similar length (25 mm).

4 Experimental results and discussion

4.1 Laser Intensity

The effect of laser excitation intensity on CPT resonance is studied by measuring transmitted laser light through the vapor cell at different incident intensities while maintaining the vapor cell at constant temperature. Fig. 5 shows the variation of FWHM with incident laser intensity, measured in vapor cells with radius, R = 12.5 mm, 7.5 mm and 5 mm. It can be observed that the FWHM is increasing linearly with laser intensity which is in agreement with the theoretical fitting (solid line) as per Eq. (1).

The intercepts of these linear curves at I_L = 0 (Fig. 5) represents the minimum linewidth of CPT resonance, *i.e.*, $\Delta\nu_{LT} = \frac{\gamma_2}{\pi} = 220.48$ Hz, 286.55 Hz and 311.74 Hz for cells with radius R=12.5 mm, 7.5 mm and 5 mm, respectively. These values indicate the lower limit of FWHM under the experimental conditions (*i.e.*, choice of cell dimension, temperature, buffer gas etc.). $\Delta\nu_{LT}$ is higher for cells with smaller radius. This is due to the higher ground state relaxation rate (γ_2) as a result of enhanced atom-wall collisions in cells with smaller dimension which would affect the coherence. The slope and intercept at I_L = 0 from experimental data shown in Fig. 5 are used to derive γ_2 and Γ^* values which are further used in the theoretical computation of CPT resonances as shown in Fig. 2.

For each incident laser excitation intensity, the Rabi frequency of the transmitted laser light is calculated at the exit of the vapor cell (L=25 mm) using the theoretical model as explained above. This estimated Rabi frequency when plotted as function of Raman detuning represents the CPT resonance as shown in Fig. 2. The quality figure (q) of the corresponding CPT resonance is extracted by performing Lorentzian fit. Fig. 6 shows the plot of q (computed as well as experimental) with incident laser intensity. The trend in the variation of measured values of q with excitation intensity is in line with the theoretical predictions (also see the variation of q for cell with L = 25 mm in Fig. 3). Further, the quality figure decreases with decrease in cell size (radius) due to higher FWHM among lower dimension cells. As

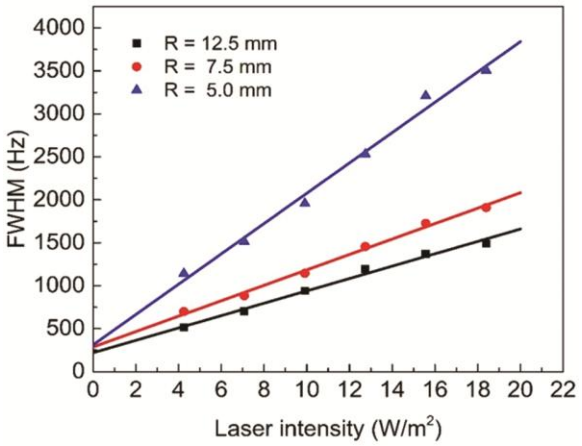

Fig. 5 — Measured linewidth of CPT resonance (FWHM) as function of incident laser excitation intensity and its corresponding linear fit (solid line) for vapor cells with radii, R = 12.5 mm, 7.5 mm and 5.0 mm @ temperature, T = 71 ^{o}C.

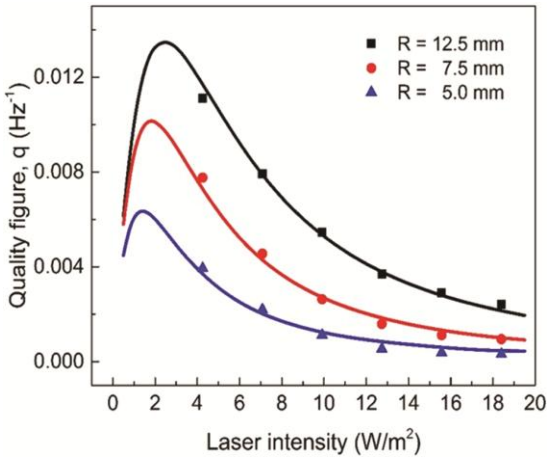

Fig. 6 — Variation of measured (experimental) quality figure of CPT resonance with respect to incident laser intensity for three cells with radius, R = 12.5 mm (square), 7.5 mm (circle) and 5 mm (triangle) all kept at temperature, T = 71 ^{o}C. Solid lines are computed from theoretical model using Eq. (6).

seen in Fig. 6, although the quality figure improves by lowering the laser excitation intensity, measurement of CPT resonances at lower intensities requires more sensitive detection scheme. In our experiment, the optimum laser intensity with maximum quality figure is 4.25 W/m^2 for the cell with radius, R = 12.5 mm. Nevertheless, the computation of theoretical values is extended to even further lower intensities and it is observed that the quality figure deteriorates below an optimum laser intensity as shown in Fig. 6.

4.2 Cell Temperature

The amplitude of CPT resonance, *i.e.*, its contrast, depends on Rabi frequency and atomic number

density which varies with temperature (T). In this regard, effect of cell temperature on the characteristics of CPT resonance is studied experimentally among Rb cells with different radius. In our experiment, the cell temperature was stabilized to a chosen value within a tolerance of ±0.01 ^{0}C.

Fig. 7 shows the FWHM as function of cell temperature at a laser excitation intensity of 7.08 W/m^2 for cells with three different dimensions. FWHM is higher for lower dimension cells due to increase in wall collisions which destroy the coherence. For a given cell size, FWHM decreases marginally with increase in temperature. Higher cell temperature enhances collision between Rb-Rb atoms as well as Rb-buffer gas. The higher Rb-Rb collision rate would result in increase in FWHM of CPT resonance. On the other hand, the higher Rb-buffer gas atoms collision results in tighter confinement of the Rb atoms in the probing volume which will lead to increase in the transit time thereby reducing the FWHM. The net reduction in the FWHM observed in our experiment indicates that Rb-buffer gas collision is influencing the behaviour of CPT resonance characteristics more strongly under these operating conditions, particularly the temperature range. Moreover, similar variation of FWHM with respect to temperature is also reported in Ref. (21). In addition, the rate of reduction in FWHM is more in cell with lower dimension due to stronger confinement effect with increase in temperature.

Fig. 8 shows variation of q and the corresponding contrast (inset) with cell temperature for three cells. In each cell, the contrast increases with temperature and reaches a maximum value (C_{pk}) beyond which it decreases with temperature[5,6,22,23]. We define the temperature at which the contrast is maximum as *Optimum Temperature* (T_{opt}) which is function of cell dimension (R) and laser excitation intensity (I_L). For $T < T_{opt}$, as the temperature increases, more and more atoms (n_{Rb} varies as T) are available for interaction with the laser field which results in higher contrast. At $T > T_{opt}$, the contrast reduces with increase in temperature owing to the ravaging contribution from number density dependent mechanisms such as increase in optical thickness of medium and enhanced spin exchange collision[5-7,14,21,22]. Therefore, at higher temperatures, the absorption of light increases along the length of vapor cell due to increase in optical thickness that leads to reduction in contrast. In addition, the higher number density at elevated temperatures ($T > T_{opt}$) induces more single photon absorption between the hyperfine levels thereby quenching the two-photon resonance transition that excites the CPT phenomena. This leads to reduced contrast at higher cell temperatures. Further, more experiments are needed to understand these dynamics.

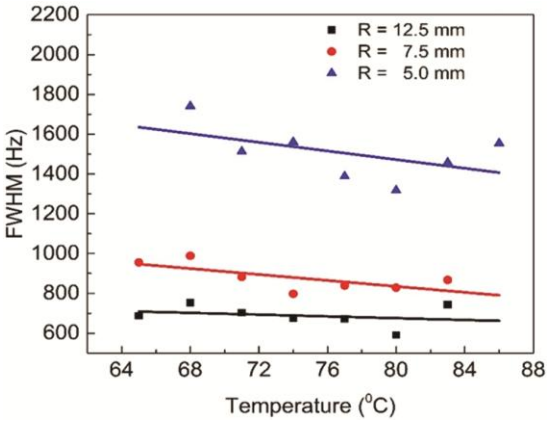

Fig. 7 — Measured FWHM of CPT resonance as function of temperature in cells with radius, R = 12.5 mm (squares), 7.5 mm (circles) and 5 mm (triangles) at a laser excitation intensity of 7.08 W/m^2. FWHM is higher among lower dimension cells. Here, the solid lines are the corresponding linear fit to guide the eye.

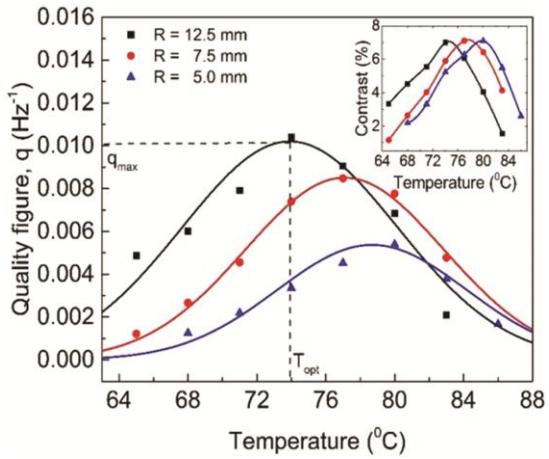

Fig. 8 — Measured quality figure as function of temperature for three cells with radius, R = 12.5 mm (squares), 7.5 mm (circles) and 5 mm (triangles) at a laser intensity of 7.08 W/m^2. The solid curves indicate the Gaussian fit to the experimental data. Inset: The corresponding CPT resonance contrast as function of temperature.

For a given cell dimension, the variation in the magnitude of q with temperature is primarily determined by changes in contrast which exhibits characteristic temperature dependent peak at T_{opt} as explained above. However, when compared among cells with different dimensions, T_{opt} shifts to higher temperature for lower dimension cells while magnitude of q_{max} at T_{opt} decreases whereas magnitude of corresponding contrast at T_{opt} is similar for all the

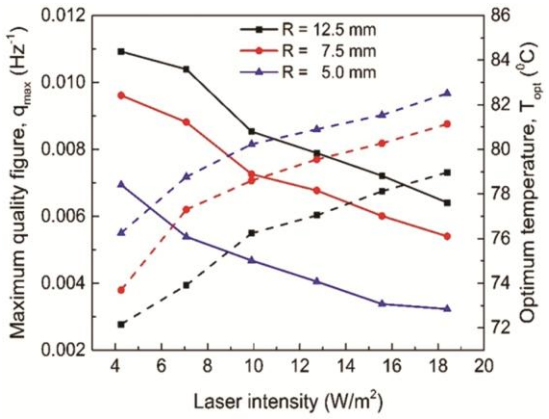

Fig. 9 — The plot of the maximum quality figure, q_{max}, (solid lines, left y-axis) of CPT resonance and corresponding optimum temperature, T_{opt}, (dashed lines, right y-axis) as function of laser excitation intensity for cells with radius, R = 12.5 mm, 7.5 mm and 5 mm.

Table 1 — Fitting parameters for the fitting curves in Fig. 8.

Cell Radius (mm)	q_{max} (Hz^{-1})	T_{Opt} (^{o}C)	T_w (^{o}C)
12.5	1.0E-2	73.93	5.66
7.5	8.9E-3	77.15	5.19
5	5.3E-3	78.58	5.04

cells. The reduction in overall magnitude of q among lower dimension cells is attributed to the increased FWHM (see Fig. 7). For a given temperature, the effect of wall collision is more for cells with lower dimension. The increase in temperature influences the confinement time of the atoms within the laser beam, thereby minimizing the detrimental role of wall collision. Thus, to achieve similar contrast value as in larger cells, the temperature of smaller cells would need to be increased which results in higher optimum temperature (T_{opt})[5].

The solid curves shown in Fig. 8 are the fit to measured data points using Gaussian function as given in Eq. (8)

$$q(T) = q_{max} \,.\, exp[-\frac{1}{2}\left(\frac{T - T_{Opt}}{T_w}\right)^2] \qquad \ldots(8)$$

where fitting parameter q_{max} is the optimum q value, *i.e.*, the peak amplitude of quality figure at T_{opt} and T_w represents the peak width (1-sigma). The values of fitting parameters for the curves shown in Fig. 8 are provided in Table 1. Amplitude of q_{max} reduces with decrease in cell dimension due to increase in FWHM as shown in Fig. 7. The optimum q value is maximum for cell with higher dimension. Thus, cells with larger radius are ideal for realizing CPT with optimized resonance characteristics which in turn helps in improving the frequency stability of atomic clock.

The peak value of contrast, C_{pk}, hence, q_{max} and its corresponding temperature, T_{opt}, also depend on laser intensity[21,24]. Fig. 9 depicts the variation of fit value of q_{max} and its corresponding T_{opt} as function of laser excitation intensity for three cell dimensions. It is clear that the value of q_{max} is higher for cells with higher dimension and lower excitation intensity.

5 Conclusion

An experimental investigation is carried out to study the dependence of quality figure (q) value on critical operating parameters such as laser excitation intensity and cell temperature as well as its dimension. CPT resonance and its corresponding q are modelled with respect to cell length and radius using a four-level atomic system by introducing a scaling parameter (β) to account for the cell size (radius) which would reflect the influence of collisional dynamics, particularly wall collision. Further, for a given cell radius the q value decreases with increase in laser intensity which is in good agreement with the theoretical model. Our study shows that the optimum temperature (T_{opt}) that corresponds to maximum q value (q_{max}) depends on laser excitation intensity as well as cell dimension (radius). This study is useful in understanding light absorption, collisional dynamics in atomic vapor cell and optimization of operating parameters of CPT based atomic clock. Finally, the optimized quality figure achieved in our study, *i.e.*, q_{max} ~ 0.01 Hz^{-1}, would enable the stabilization of clock frequency to a level better than 2 x 10^{-12} per sec.

Acknowledgments

The authors would like to thank Mr. N. Thakur, Mr. M. M. Mehra, Mr. P. Selvaraj and A. S. Laxmiprasad (all at LEOS, ISRO, Bangalore) for their valuable suggestions. K. Rajaiah would like to acknowledge Mrs. S. Nirmala and Mr. A. Kartik from Space Navigation Group, U.R. Rao Satellite Centre, ISRO, Bangalore for their support and encouragement. This work is supported and funded by Indian Space Research Organisation (ISRO), India.

References

1 Merimaa M, Lindvall T, Tittonen I & Ikonen E, *J Opt Soc Am B*, 20 (2003) 273.

2 Kitching J, Knappe S & Vukicevic N, *et al.*, *IEEE Trans Instrument Meas*, 49 (2000) 1313.

3 Vanier J, *Appl Phys B: Lasers Opt*, 81 (2005) 421.
4 Vanier J, Levine M W, Janssen D & Delaney M J, *IEEE Trans Instrument Meas*, 52 (2003) 822.
5 Knappe S, Kitching J, Hollberg L & Wynands R, *Appl Phys B*, 74 (2002) 217.
6 Deng J, Zheng H, Hui H & Wang Y, *Chinese Phys Lett*, 23 (2006) 1745.
7 Boudot R, Dziuban P, Hasegawa P M, *et al., J Appl Phys*, 109 (2011) 014912.
8 Vanier J, Godone A & Levi F, *Phys Rev A*, 58 (1998) 2345.
9 Wynands R & Nagel A, *Appl Phys B*, 68 (1999) 1.
10 Lindvall T, Merimaa M, Tittonen I & Ikonen E, "All-optical atomic clock based on dark states of ^{85}Rb", *Proc of the 6th Symp on Freq Stds and Metrology* (2002).
11 Micalizio S, Godone A, Levi F & Vanier J, *Phys Rev A*, 73 (2006) 033414.
12 Vanier J & Audoin C, The Quantum Physics of Atomic Frequency Standards, Bristol, U K: Adam Hilger, (1989).
13 Siddons P, Adams C S, Ge C & Hughes I G, *J Phys B: At Mol Opt Phys*, 41 (2008) 155004.
14 Knappe S, Wynands R, Kitching J, *et al*, *J Opt Soc Am B*, 18 (2001) 1545.
15 Moon H, Park S, Park Y, *et al*, *J Opt Soc Am B*, 23 (2006) 2393.
16 Vanier J, Levine M W, Janssen D & Delaney M, *Phys Rev A*, 67 (2003) 065801.
17 Steck D A, Rubidium 87 D Line Data, http:// steck.us/alkalidata (2019).
18 Godone A, Levi F, Micalizio S & Vanier J, *Eur Phys J D*, 18 (2002) 5.
19 Shah V & Kitching J, *Adv Atom Molecul Opt Phys*, 59 (2010) 21.
20 Miletic D, Affolderbach C, Hasegawa M, *et al*, *Appl Phys B*, 109 (2012) 89.
21 Yun P, Tricot F & Calosso C E, *et al*, *Phys Rev Appl*, 7 (2017) 014018.
22 Castagna N, Boudot R, Guerandel S, *et al*, *IEEE Trans Ultra Ferroelect Freq Control*, 56 (2009) 246.
23 Micalizio S & Godone A, *Phys Rev A*, 99 (2019) 043425.
24 Kozlova O, Danet J, Guérandel S & Clercq E, *IEEE Trans Instrument Meas*, 63 (2014) 1863.